fronts [38], and stationary bumps [39] can all be analyzed in stochastic neural Þelds with the aid of small-noise expansions originally developed to analyze wave propagation in stochastic partial differential equations [40]. Such an approach typically results in a diffusion equation for the position of the spatiotemporal activity, but upon considering a neural Þeld with multiple layers, the effective equations are multivariate Orstein-Uhlenbeck (OU) processes instead [30]. Thus, the perturbation expansion allows one to examine the effects of connectivity between layers, in addition to noise. Since recordings of cortical activity are becoming substantially more detailed [3,4], the time is ripe for extending theories of spatiotemporal activity patterns in cortex.

We extend our previous work from [30] in several ways. First of all, our analysis of deterministic systems with laminar structure analyzes the effect of arbitrarily strong coupling upon the propagation speed of waves and the width of traveling pulses. Interlaminar coupling increases (decreases) the speed of waves in the case of fronts (pulses). In addition, we Þnd that such a shift in wave speed appears in the weak coupling calculations we perform in the case of the stochastic neural Þeld. This is due to reßections and, for pulses, the synaptic connectivity function no longer being reßection symmetric. We also note that, in the case of traveling fronts, we explore the effect of noise correlation lengths upon the effective diffusion of waves. Our Þndings suggest noise with longer correlation length leads to higher diffusion, and thus more irregular wave propagation. Finally, we remark that our results show that our perturbation analysis provides accurate asymptotic results for propagating waves, in addition to stationary bumps.

The paper will proceed as follows. In Sec. II, we introduce the models we explore, showing how noise and a multilaminar structure can be introduced into neural Þeld models [35]. One important point is that the correlation structure of spatiotemporal noise can be tuned in the model, and changing this has nontrivial effects on the resulting dynamics. We proceed, in Sec. III, to show how a combination of interlaminar connectivity along with noise affects the propagation of traveling fronts in an excitatory neural Þeld model. As in [30], we are able to derive an effective equation for the position of the front, which takes the form of a multivariate OU process. Finally, we derive similar results for traveling pulse propagation in asymmetric neural Þelds in Sec. IV.

where $u_j(x,t)$ is the neural activity of population $j$ at $x \in$ and at time $t$, and the effects of synaptic architecture are described by the convolution

$$w_{jk}$$

## II. LAMINAR NEURAL FIELD MODEL

We will consider two different models for wave propagation in neural Þelds. They both take the form of a system of coupled stochastic neural Þeld equations

$$du_1(x,t) = \left[ -u_1 + \sum_{k=1}^{2} w_{1k} * f(u_k) \right] dt + \epsilon^{1/2} dW_1(x,t),$$

(1a)

$$du_2(x,t) = \left[ -u_2 + \sum_{k=1}^{2} w_{2k} * f(u_k) \right] dt + \epsilon^{1/2} dW_2(x,t),$$

(1b)

so excitatory coupling ($w_c > 0$) between layers increases the speed $c$ of both fronts. Finally, in the limit $w_c \to 0$, there are two decoupled fronts, both with speed $c = 1/(2\theta) - 1$. This is the limit from which we will build our theory of stochastically driven coupled fronts.

In the limit $w_c \to 0$, the fronts (12) are neutrally stable to perturbations in both directions. To see this, we consider the perturbed front solutions $u_j(x,t) = U_j(\xi) + \psi U_j(\xi)e^{\lambda t}$, plugging into (1) and truncating to linear order with $w_{11} = w_{22} = w$ and $w_{12} = w_{21}$

FIG. 1. (Color online) (a) Speed $c$ and (b) position parameter $a$ of coupled traveling fronts (12) as determined by the implicit system (13). Notice $a = 0$ when $w_{21} = w_{12}$. Threshold $\theta = 0.4$.

FIG. 2. (Color online) Evolution of coupled fronts (12) in space-time. (a) When $w_{12} = w_{21} = 0.1$, fronts propagate at the same speed with the same threshold crossing point $x_c(t)$ (solid line), where $u_1(x_c(t),t) = u_2(x_c(t),t) = \theta$. (b) When $w_{12} = 0.1$ and $w_{21} = 0.01$, the crossing point $x_1(t)$ of the front in the first layer $u_1(x_1(t),t) = \theta$ (solid line) stays ahead of the crossing point $x_2(t)$ (dashed line) of the front in the second layer $u_2(x_2(t),t) = \theta$.
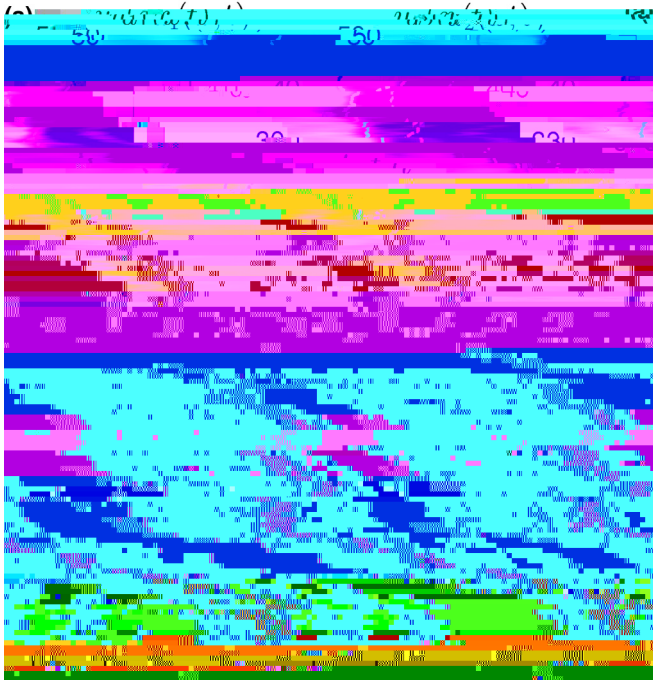
FIG. 3. (Color online) (a) Uncoupled fronts $u_1$ and $u_2$ propagating in the dual layer stochastic neural field have leading edges (solid and dashed lines, respectively) that spread apart due to separate

where the associated diffusion coefficients of the variance are

$$D_j = \frac{\int_{-\infty}^{\infty}\int_{-\infty}^{\infty} \varphi_j(x)\varphi_j(y)C_j(x-y)\,dx\,dy}{\left[\int_{-\infty}^{\infty}\varphi_j(x)U_j'(x)\,dx\right]^2}, \qquad (28)$$

for $j = 1,2$, and covariance is described by the coefficient

$$D_c = \frac{\int_{-\infty}^{\infty}\int_{-\infty}^{\infty} \varphi_1(x)\varphi_2(y)C_c(x-y)\,dx\,dy}{\left[\int_{-\infty}^{\infty}\varphi_1(x)U_1'(x)\,dx\right]\left[\int_{-\infty}^{\infty}\varphi_2(x)U_2'(x)\,dx\right]}.$$

With the stochastic system (27) in hand, we can show how coupling between layers affects the variability of the positions of fronts subject to noise. To do so, we diagonalize the matrix $K = V \Lambda V^{-1}$ with right eigenvector matrix

$$V = \begin{pmatrix} 1 & \kappa_1 \\ 1 & -\kappa_2 \end{pmatrix},$$

and $\Lambda = \mathrm{diag}(\lambda_1,\lambda_2)$. Front positions $(\epsilon_1,\epsilon_2)^T$ are neutrally stable ($\lambda_1 = 0$) to perturbations in the same direction $v_1 = (1,1)^T$ and stable [$\lambda_2 = -(\kappa_1+\kappa_2)$] to perturbations in opposite directions $v_2 = (\kappa_1, -\kappa_2)^T$.

We now show how coupling leads to a time-varying mean in $\Delta(t)$ as opposed to the case of bumps [36]. With the diagonalization $K = V\Lambda V^{-1}$, assuming $\Delta(0) = 0$, the mean $\langle\Delta(t)\rangle = \int_0^t e^{K(t-s)}ds\,J$, so

$$\langle\Delta\rangle = \begin{pmatrix} \mathcal{A}t + \mathcal{B}\kappa_1(1 - e^{-(\kappa_1+\kappa_2)t}) \\ \mathcal{A}t - \mathcal{B}\kappa_2(1 - e^{-(\kappa_1+\kappa_2)t}) \end{pmatrix},$$

where $\mathcal{A} = \frac{\kappa_1 J_2 + \kappa_2 J_1}{\kappa_1+\kappa_2}$, $\mathcal{B} = \frac{J_1 - J_2}{(\kappa_1+\kappa_2)^2}$, and we have used the diagonalization $e^{Kt} = Ve^{\Lambda t}V^{-1}$. Since $\lambda_2 = -(\kappa_1+\kappa_2) < 0$,

$$\lim_{t\to\infty} \langle\Delta(t)\rangle = \begin{pmatrix} \mathcal{A}t + \mathcal{B}\kappa_1 \\ \mathcal{A}t - \mathcal{B}\kappa_2 \end{pmatrix},$$

so the net mean effect of weak coupling is to slightly increase the wave speed ($\mathcal{A}t$) and potentially alter the relative position of the fronts ($\mathcal{B}$). We would expect this, based on the speeding up of fronts observed in our deterministic analysis. Note that if $\kappa_1 = \kappa_2$, then $\mathcal{B} = 0$ and the fronts will have the same mean position.

To understand the collective effect that noise and coupling

using (12) (see also [46,47]):

$$U_j(\cdot) = \begin{cases} e^{\check{S}} : & > 0 \\ 1\,\check{S}\,\frac{(1\check{S}2\,)^2}{1\check{S}4}e^{\frac{2}{1\check{S}2}} + \frac{e}{1\check{S}4} : & < 0 \end{cases} \qquad (33)$$

and we differentiate (33) to yield

$$U_j(\cdot) = \begin{cases} \check{S}\,e^{\check{S}} : & > 0 \\ \check{S}\,\frac{2\,(1\check{S}2\,)}{1\check{S}4}e^{\frac{2}{1\check{S}2}} + \frac{e}{1\check{S}4} : & < 0. \end{cases} \qquad (34)$$

Now, we can solve explicitly for the null vectors of . Plugging (33) and (34) into (21), and using the derivative
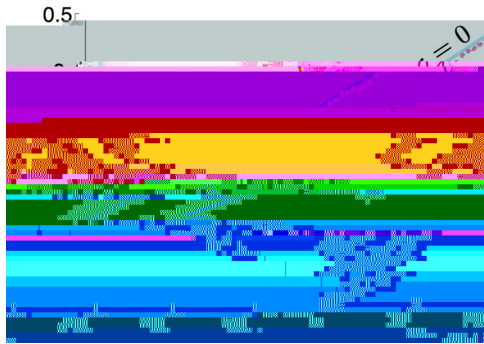
$$\frac{d}{dU}H\,[U$$

FIG. 5. (Color online) Effects of cosine correlated noise $[C_j(x) = \cos(x)]$ on propagation of coupled fronts. Theory given by (41). As the strength of identical reciprocal coupling $\beta_1 = \beta_2 = \beta$ is increased, the variance of front position $\Delta_1(t)$ (

Thus, we can integrate the two equations (46) and apply the threshold conditions $U_1$

FIG. 9. Pulse width $a_1 = a_2 = a$ as a function of the asymmetry of the local weight functions $w_1(x) = w_2(x) = \cos(x - \sigma)$ for varying amplitudes of reciprocal symmetric strength $w_{12} = w_{21} = w_c$. Increasing the strength $w_c$ shifts the saddle-node bifurcation, at which the stable (solid) and unstable (dashed) branches of pulse solutions, to the right in . Other parameter $\theta = 0.4$.

neuronal network that supported fronts. Essentially, perturbations must obey (15), which has an eigenvalue $= 0$ associated with the eigenfunction $U_j'$ for each layer $j = 1,2$. As in the case of traveling fronts, coupled pulses are still neutrally stable to perturbations that move them in the same direction. However, we will now show that coupling layers stabilizes pulses to perturbations that pull them in opposite directions.

### B. Noise-induced motion of coupled pulses

Now, we analyze the effects of weak noise on the propagation of pulses in the presence of reciprocal coupling that is weak [$w_{12}, w_{21} = O(\epsilon^{1/2})$] and local coupling that is identical ($w_{11} = w_{22} = w$). To start, we presume noise causes each pulseÕs position to wander, described by stochastic variables $\Delta_1(t)$ and $\Delta_2(t)$, and each pulseÕs proÞle ßuctuates, described by the stochastic variables $\Phi_1(x,t)$ and $\Phi_2(x,t)$. As in the case of coupled traveling fronts, this is described by the expansion given by the ansatz (28). Plugging this into (1) and expanding in powers of $\epsilon^{1/2}$, we Þnd the pulse solution at $O(1)$ where $w_{12} = w_{21} \equiv 0$. At $O(\epsilon^{1/2})$, we Þnd the system (19) with associated linear operator $\mathcal{L}$ given by (20), as we found for the excitatory network with fronts. Next, we apply a solvability condition to (19), where the inhomogeneous part must be orthogonal to the null space of

$$\mathcal{L}^* \, p = \begin{pmatrix} -c\,\partial_x p + f'(U_1)[w(-x) * p(x)] \\ -c\,\partial_x q + f'(U_2)[w(-x) * q(x)] \end{pmatrix}, \quad (53)$$

where $p = (p(x),q(x))^T$. It is important to note that an asymmetric weight function $w(x)$, like (3), leads to a slightly different form for $\mathcal{L}^*$, now involving terms such as $w(-x) * p(x) = \int_{-\infty}^{\infty} w(y - x)p(y)\,dy$. Again, we can decompose the null space of $\mathcal{L}^*$ into two orthogonal elements that take the forms $(\varphi_1,0)^T$ and $(0,\varphi_2)^T$. Rearranging the resulting solvability condition shows that the stochastic vector $\Delta(t) = (\Delta_1(t), \Delta_2(t))^T$ obeys the multivariate Ornstein-Uhlenbeck
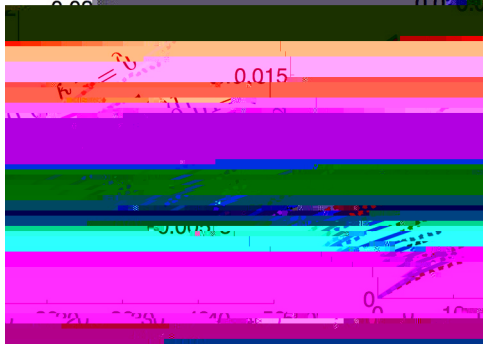
FIG. 10. (Color online) Effects of cosine correlated noise $[C_j(x) = \cos(x)]$ on propagation of coupled pulses. Theory (solid line) computed using (58) matches numerical computations (dashed line) fairly well. As the strength of identical reciprocal coupling $\kappa_1 = \kappa_2 = \kappa$ is increased, the variance of pulse position $\langle \Delta_1(t)^2 \rangle$

two-dimensional space. Our analysis could then lend insight into the neural architecture that leads to the most faithful representation of an animalÕs present position.